International Journal of Mechanics and Applications 2016, 6(3): 49-62
DOI: 10.5923/j.mechanics.20160603.03

# Stability Analysis of Model Regenerative Chatter of Milling Process Using First Order Least Square Full Discretization Method

**Ezugwu Chinedu A. K.[1], Okonkwo Ugochukwu C.[2,*], Sinebe Jude E.[3], Okokpujie Imhade P.[2]**

[1]Landmark University, Omu-Aran, Nigeria
[2]Department of Mechanical Engineering, Nnamdi Azikiwe University, Awka, Nigeria
[3]Department of Mechanical Engineering, Delta State University, Oleh Campus, Nigeria

**Abstract** Regenerative chatter is an instability phenomenon in machining operation that must be avoided if high accuracy and greater surface finish is to be achieved. It comes with its own consequences such as poor surface finish, low accuracy, excessive noise, tool wear and low material removal rate (MRR). In this paper, an analytical method base on first order least square approximation full-discretization method is use for the stability analysis on the plane of axial depth and radial depths of cut. A detail computational algorithm has been developed for the purpose of delineating stability lobe diagram into stable and unstable regions using mathematical models. These algorithms enabled the performance of sensitivity analysis. From the results axial depth of cut enhances the unstable region and suppresses the stable region. This means that inverse relationship exists between the axial and limiting radial depths of cut thus highlighting the need to determine the maximum value of their product for achieving maximized MRR thereby reducing the chatter in the milling process. It is also seen that the peak radial depths of cut occasioned by the lobbing effects occur at fixed spindle speeds irrespective of the axial depth of cut. Similarly, the rise in spindle speed enhances the stable region and suppresses the unstable region. This means that for us to have chatter-free milling process, parameters like axial and radial depths of cut should be carefully selected together at high machining speed. With these behaviour, one can locate the productive spindle speed at which the lobbing effects occur and depths of cut combination for the operator.

**Keywords** Delineation, Regenerative chatter, Full discretization, Stability lobs diagram, Milling

## 1. Introduction

Milling is an intermittent process in which shock loads are associated with both engagement and disengagement of the teeth with the workpiece [1]. Milling machine is widely used for the higher material removal rate (MRR) operating at very high speed [2]. Because of high speed, dynamic problem occurs in milling machine spindle and tool. As there is relative motion between tool and work piece, various internal and external forces rises in tool and work piece. These forces set up vibration in machine part which is in motion or in rest. Basically three types of vibration occur in machine, free vibration, forced vibration and self-excited vibration [3]. First two vibrations can be easily detected and controlled by using dampers and by other means. But, mainly chatter prediction is major task for the operator while operating at higher speed. It has a very poor surface finish which directly decreases the productivity [4].

The recent trends in manufacturing industry have an expanding requirement for enhanced characterization of cutting tools for controlling vibration and chatter amid the processing procedure [5]. The chatter is a self-excitation phenomenon happening in machine tools, in which the cutting process tends to diminish the machine structural damping resulting in an unstable condition [1]. Though chatter prediction is tough task, the area of interest in this work is to identify how the effect of regenerative chatter can be felt in pocket milling through the delineation of the stability lobs. Chatter is broadly classified in two categories: Primary chatter and secondary chatter. Primary chatter is sub classified as frictional chatter, thermo-mechanical chatter and mode-coupling chatter. Primary chatter is because of the friction between tool and work piece and it diminish with the increase in spindle speed. And secondary chatter is because of the regeneration of waviness of the surface of the work piece [6]. This chatter is called as regenerative chatter. This chatter is also known as self-excited chatter. It is very difficult to avoid regenerative chatter as it increases with the increase in spindle speed and depth of cut. Regenerative

* Corresponding author:
cu.okonkwo@unizik.edu.ng (Okonkwo Ugochukwu C.)
Published online at http://journal.sapub.org/mechanics

effect is a concept used to explain the sustained vibration occurring during machining as resulting from cutting force variation due to vibration induced surface waviness. Arnold first suggested regenerative effects as the potential cause of chatter and is now arguably considered the cause of detrimental type of machine tool vibration (Davies et al, 1999).

Chatter is the most obscure and delicate of all problems facing the machinist [7]. The first stability analysis on regenerative chatter for the orthogonal cutting process was discovered by Tobias [8] and Tlusty [9]. They obtained stability lobe diagram (SLD) on the basis of stability analysis. It shows the boundary between stable an unstable cut. By using SLD, operator may select chatter free operations for the milling machine. A detailed discussion can be seen in many papers regarding SLD. Chatter vibration has various negative effects such as:

- Poor surface quality and unacceptable accuracy,
- Tool wear and tool damage,
- Excessive noise,
- Low material removal rate (MRR),
- Low productivity rate.

## 2. Phenomenon of Regenerative Chatter

The milling process is most pronounced if the material removal rate is large enough while maintaining a high quality level [10]. The topmost limitation in machining productivity and part quality are the instability phenomenon that is frequently witness in cutting operations called regenerative chatter [11, 12]. The chatter vibrations of machine tool occur due to a self-excitation mechanism in the generation of chip thickness during machining operations. Due to the cutter vibrations a wavy surface is left on the surface of the workpiece by means of a tooth of cutter [13]. Then the very next tooth strikes the wavy surface and generates the new wavy surface as can be seen in the figure. 1 bellow. The phase difference between the two wavy surfaces varies the chip thickness. This increase the cutting forces of cutter. Then system becomes unstable, and chatter vibrations grow until the tool jump out of the cut which results in non-smooth surface. Thus if the chatter vibrations continue the material removal rate will be greatly affected [9].

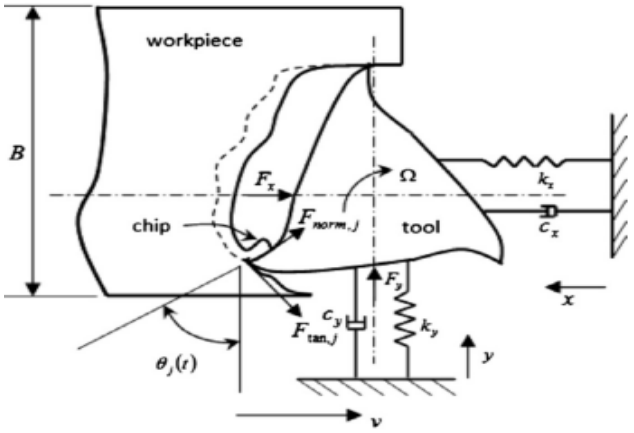


**Figure 1.** Regenerative wave milling model

## 3. Milling Chatter Model

Two degree of freedom milling model is the form of milling model chosen for this work more and this is because of lack of rigidity of the tool in its transverse plane causing compliance in both the feed and normal to feed directions.

The free-body diagram for the tool dynamics when the motion of the tool $x(t)$ is considered to be a summation of feed motion and vibrations is as shown in Fig. 2.

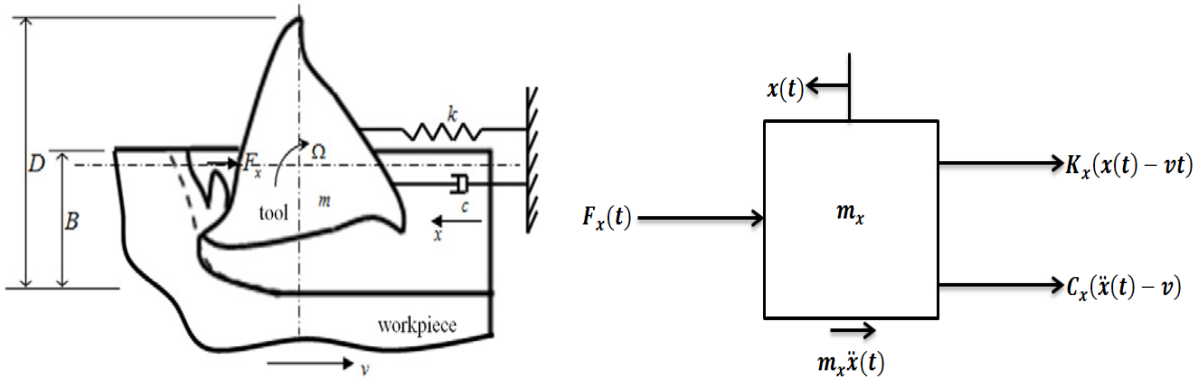


**Figure 2.** (a) 1-DOF dynamic model (b) Free-body diagram of tool dynamics

The differential equation governing the motion of the tool as seen from the free-body diagram above now becomes

$$m\ddot{x}(t) + c[\dot{x}(t) - v] + k[x(t) - vt] + Fx(t) = 0 \quad (1)$$

A tool-workpiece disposition is considered for the $jth$ tooth of the tool. The cutting force is considered as having normal and tangential components designated $F_{n,j}(t)$ and $F_{t,j}(t)$ respectively. Axial component of cutting force is neglected because helix angle is considered zero. The $x$ −component of cutting force for the tool thus becomes

$$F_x(t) = \sum_{j=gj}^{N}(t)\left[F_{n,j}(t)sin\theta_j(t) + F_{t,j}(t)cos\theta_j(t)\right] \quad (2)$$

The cutting forces on $jth$ tooth are given by the non-linear law as follows

$$F_{t,j}(t) = c_t w[f_a sin\theta_j(t)]^{\gamma} \quad (3a)$$

$$F_{n,j}(t) = c_n w[f_a sin\theta_j(t)]^{\gamma} = xF_{t,j}(t) \quad (3b)$$

The symbols $C_{\mathrm{t}}$ and $C_{\mathrm{n}}$ are the tangential and normal cutting coefficients which are numerically influenced by workpiece material properties and tool shape. The symbol $N$ stands for the number of tool teeth. Where $w$ is the depth of cut, $x$ is the ratio of $c_n/c_t$, $f_a$ is the actual feed given as $x(t) - x(t-\tau)$ which is the difference between present and one period delayed position of tool and $\gamma$ is an exponent that is usually less than one, having a value of ¾ for the three-quarter rule. The instantaneous angular position of $j$th tooth $\theta_j(t)$ is given as

$$\theta_j(t) = \left(\frac{\pi\Omega}{30}\right)t + (j-1)\frac{2\pi}{\mathrm{N}} + \alpha \quad (4)$$

where $\Omega$ is the spindle speed in rpm and $\alpha$ is the initial angular position of the tooth. The screen function $g_j(t)$ has values of either unity or nullity depending on whether the tool is cutting or not. Given start and end angles of cut $\theta_s$ *and* $\theta_e$ respectively, $g_j(t)$ becomes

$$g_j(t) = \begin{cases} 1 \; if \; \theta_s < \theta_j(t) < \theta_e \\ 0 \qquad otherwise \end{cases} \quad (5)$$

The mathematical form for $g_j(t)$ is given as

$$g_j(t) = \frac{1}{2}\left(1 + sgn\left\{sin\left[\theta_j(t) - tan^{-1}\mathcal{P}\right] - sin[\theta_s - tan^{-1}\mathcal{P}]\right\}\right) \quad (6)$$

For up milling $\theta_s \; and \; \theta_e$ are expressed in terms of radial depth of cut $b$ [22]

$$\theta_s = \begin{cases} 0 & Up - milling \\ \cos^{-1}(2\,b/D - 1) & Down - milling \end{cases} \quad (7a)$$

$$\theta_e = \begin{cases} \cos^{-1}(1 - 2\,b/D) & Up - milling \\ \pi & Down - milling \end{cases} \quad (7b)$$

Figure 3 below is a 2 DOF depiction of an end-milling tool, with the stiffness and damping elements oriented in the $x-y$ plane (horizontal plane). The modal parameters $k_x, m_x$ and $c_x$ are for $x-$vibration while $k_y, m_y$ and $c_y$ are for $y-$vibration

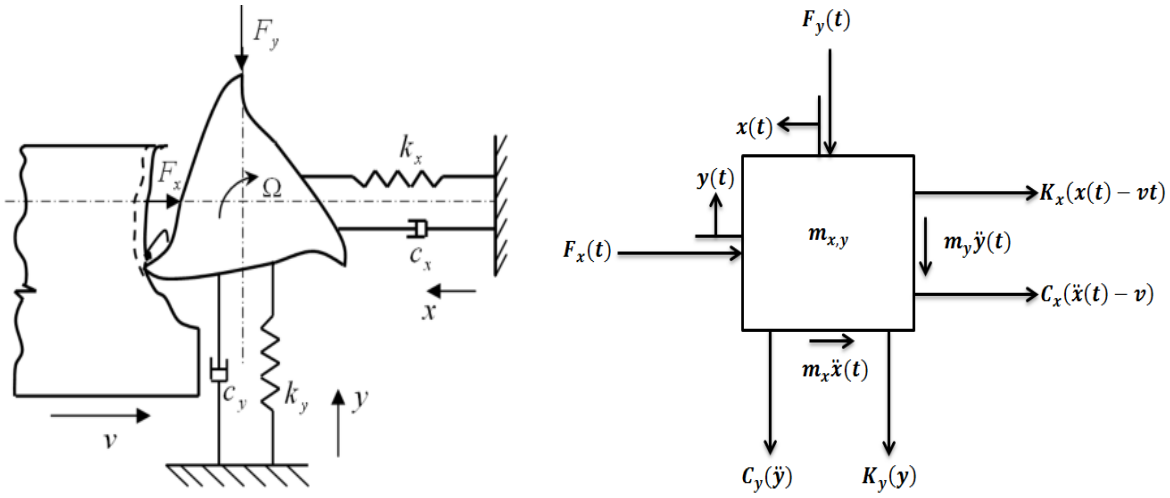


**Figure 3.** (a) 2-DOF tool dynamics (b) Free-body diagram of toll dynamics

The governing equation of motion now becomes

$$m_x\ddot{x}(t) + c_x[\dot{x}(t) - v] + k_x[x(t) - vt] + F_x x(t) = 0 \quad (8a)$$

$$m_y\ddot{y}(t) + c_y\dot{y}(t) + ky(t) + F_y(t) = 0 \quad (8b)$$

The $x$ and $y-$component of the cutting force on the tool are

$$F_x(t) = \sum_{j=gj}^{N}(t)\left[F_{n,j}(t)sin\theta_j(t) + F_{t,j}(t)cos\theta_j(t)\right] \quad (9a)$$

$$F_y(t) = \sum_{j=gj}^{N}(t)\left[-F_{n,j}(t)cos\theta_j(t) + F_{t,j}(t)sin\theta_j(t)\right] \quad (9b)$$

The actual feed rate $f_a$ of $jth$ tooth at angular position $\theta_j(t)$ is given as

$$f_a(t) = [X(t) - x(t-\tau)]sin\theta_j(t) + [Y(t) - y(t-\tau)cos\theta_j(t) \tag{10}$$

where $X(t) = vt + x_t(t) + x(t), Y(t) = y_t(t) + y(t)$.

The quantity $x(t)$ and $y(t)$ are perturbations in the $x$ and $y$ −directions respectively.

The linearized Taylor series expansion of ${f_a}^{\gamma}$ about $v\tau sin\theta_j(t)$ then reads

$${f_a}^{\gamma} = [v\tau sin\theta_j(t)]^{\gamma} + \gamma[v\tau sin\theta_j(t)]^{\gamma-1}\{[x(t) - x(t-\tau)]sin\theta_j(t) + [y(t) - y(t-\tau)]cos\theta_j(t) \tag{11}$$

When $x(t)$ and $y(t)$ are considered to be zero in equations (11), (3a-3b) and (9a- 9b) above, we will form equations (12a) and (12b) from equations (8a) and (8b)

$$m_x\ddot{x}(t) + c_x\dot{x}_t(t) + k_x x_t(t) = -F_{px}(t) \tag{12a}$$

$$m_y\ddot{y}(t) + c_y\dot{y}_t(t) + k_y y_t(t) = -F_{py}(t) \tag{12b}$$

Where

$$F_{px}(t) = cw(v\tau)^{\gamma}\sum_{j=gj}^{N}(t)sin^{\gamma}\theta_j(t)\left[xsin\theta_j(t) + cos\theta_j(t)\right] \tag{13a}$$

$$F_{py}(t) = cw(v\tau)^{\gamma}\sum_{j=gj}^{N}(t)sin^{\gamma}\theta_j(t)\left[-xcos\theta_j(t) + sin\theta_j(t)\right] \tag{13b}$$

The periodic forces $-F_{px}(t)$ and $-F_{py}(t)$ respectively drives the two orthogonal $\tau$ −periodic tool responses $x_t(t)$ and $y_t(t)$.

Putting equations (12a-12b) into equation (8a-8b) and simplifying give

$$m_x\ddot{x}_x(t) + c_x\dot{x}_x(t) + k_x x_x(t) = -h_{xx}(t)[x(t) - x(t-\tau)] - h_{xy}(t)[y(t) - y(t-\tau)] \tag{14a}$$

$$m_y\ddot{y}_y(t) + c_y\dot{y}_y(t) + k_y y_y(t) = -h_{yx}(t)[x(t) - x(t-\tau)] - h_{yy}(t)[y(t) - y(t-\tau)] \tag{14b}$$

In the light of specific periodic cutting force variations, we have as

$$h_{xx}(t) = C_t\sum_{j=1}^{N} g_j(t)\sin\left(\theta_j(t)\right)\left[(C_n/C_t)\sin\theta_j(t) + \cos\theta_j(t)\right] \tag{15a}$$

$$h_{xy}(t) = C_t\sum_{j=1}^{N} g_j(t)\cos\theta_j(t)\left[(C_n/C_t)\sin\theta_j(t) + \cos\theta_j(t)\right] \tag{15b}$$

$$h_{yx}(t) = C_t\sum_{j=1}^{N} g_j(t)\sin\left(\theta_j(t)\right)\left[(C_n/C_t)\cos\theta_j(t) - \sin\theta_j(t)\right] \tag{15c}$$

$$h_{yy}(t) = C_t\sum_{j=1}^{N} g_j(t)\cos\theta_j(t)\left[(C_n/C_t)\cos\theta_j(t) - \sin\theta_j(t)\right] \tag{15d}$$

Equations (14a) and (14b) are put in matrix form gives

$$\ddot{\mathrm{x}}(t) + \mathrm{M}^{-1}\mathrm{C}\dot{\mathrm{x}}(t) + \mathrm{M}^{-1}\mathrm{K}\mathrm{x}(t) = \mathrm{M}^{-1}\mathrm{H}(\mathrm{t})[\mathrm{x}(t) - \mathrm{x}(t-\tau)] \tag{16}$$

Where $X(t) = \{x(t)\ \ y(t)\}^T$ is the vector of chatter vibration in the two orthogonal directions of $x$ and $y$, the mass M, damping C and stiffness K matrices are respectively given as

$$M = \begin{bmatrix} m_x & 0 \\ 0 & m_y \end{bmatrix},\ C = \begin{bmatrix} c_x & 0 \\ 0 & c_y \end{bmatrix},\ K = \begin{bmatrix} k_x & 0 \\ 0 & k_y \end{bmatrix} \tag{17}$$

The forcing function in equation (17) $H(t)X(t-\tau)$ contains a time-periodic function $H(t)$ that results from rotational motion of the milling teeth

$$H(t) = -w\begin{bmatrix} h_{xx}(t) & h_{xy}(t) \\ h_{yx}(t) & h_{yy}(t) \end{bmatrix} \tag{18}$$

By pre-multiplying equation (16) with the inverse of the mass matrix, the modal form of the governing model upon little re-arrangement becomes

$$\ddot{\mathrm{x}}(t) + \mathrm{M}^{-1}\mathrm{C}\dot{\mathrm{x}}(t) + \mathrm{M}^{-1}[\mathrm{K} - \mathrm{H}(\mathrm{t})]\mathrm{x}(t) = -\mathrm{M}^{-1}\mathrm{H}(\mathrm{t})\mathrm{x}(t-\tau) \tag{19}$$

The expanded form of equation (19) when each of the matrix operations $\mathrm{M}^{-1}\mathrm{C}$, $\mathrm{M}^{-1}\mathrm{K}$ and $\mathrm{M}^{-1}[\mathrm{K} - \mathrm{H}(\mathrm{t})]$ are carried out reads

$$\begin{Bmatrix} \ddot{x}(t) \\ \ddot{y}(t) \end{Bmatrix} + \begin{bmatrix} 2\zeta_x\omega_{nx} & 0 \\ 0 & 2\zeta_y\omega_{ny} \end{bmatrix}\begin{Bmatrix} \dot{x}(t) \\ \dot{y}(t) \end{Bmatrix} + \begin{bmatrix} \omega_{nx}^2 + \frac{wh_{xx}(t)}{m_x} & \frac{wh_{xy}(t)}{m_x} \\ \frac{wh_{yx}(t)}{m_y} & \omega_{ny}^2 + \frac{wh_{yy}(t)}{m_y} \end{bmatrix}\begin{Bmatrix} x(t) \\ y(t) \end{Bmatrix} = \begin{bmatrix} \frac{wh_{xx}(t)}{m_x} & \frac{wh_{xy}(t)}{m_x} \\ \frac{wh_{yx}(t)}{m_y} & \frac{wh_{yy}(t)}{m_y} \end{bmatrix}\begin{Bmatrix} x(t-\tau) \\ y(t-\tau) \end{Bmatrix} \tag{20}$$

Equation (20) is the model for milling chatter whose stability behaviour is of interest in this work.

# 4. Progress in Stability Analysis of Milling

Stability analysis of milling process is normally carried out on either the state space form or non-state space form of the governing model. Most stability analysis carried out on milling process using the methods of semi-discretization [14, 5], temporal finite element analysis [16] and the full-discretization method [17, 18] are formulated on the state space form of the governing model while stability analysis based on the methods of Zero order approximation or multi-frequency solution can be formulated on the non-state space version of the governing model.

Considering the governing model (equation (20)), four state variables can be identified; $x(t)$, $y(t)$, $\dot{x}(t)$ and $\dot{y}(t)$. The state variables are then designated as follows; $y_1(t) = x(t)$, $y_2(t) = y(t)$, $y_3(t) = \dot{x}(t)$ and $y_4(t) = \dot{y}(t)$. For better understanding of the process of state space transformation of equation (20), two constituent equations are written out as

$$\ddot{x}(t) + 2\zeta_x\omega_{nx}\dot{x}(t) + \left(\omega_{nx}^2 + \frac{wh_{xx}(t)}{m_x}\right)x(t) + \frac{wh_{xy}(t)}{m_x}y(t) = \frac{wh_{xx}(t)}{m_x}x(t-\tau) + \frac{wh_{xy}(t)}{m_x}y(t-\tau) \quad (21a)$$

$$\ddot{y}(t) + 2\zeta_y\omega_{ny}\dot{x}(t) + \frac{wh_{yx}(t)}{m_y}x(t) + \left(\omega_{ny}^2 + \frac{wh_{yy}(t)}{m_y}\right)y(t) = \frac{wh_{yx}(t)}{m_y}x(t-\tau) + \frac{wh_{yy}(t)}{m_y}y(t-\tau) \quad (21b)$$

In light of the identified state variables, equation (21a-21b) can be re-written as

$$\dot{y}_1(t) = y_3(t) \quad (22a)$$

$$\dot{y}_2(t) = \dot{y}(t) = y_4(t) \quad (22b)$$

$$\dot{y}_3(t) = -\left(\omega_{nx}^2 + \frac{wh_{xx}(t)}{m_x}\right)y_1(t) - \frac{wh_{xy}(t)}{m_x}y_2(t) - 2\zeta_x\omega_{nx}y_3(t) + \frac{wh_{xx}(t)}{m_x}y_1(t-\tau) + \frac{wh_{xy}(t)}{m_x}y_2(t-\tau) \quad (22c)$$

$$\dot{y}_4(t) = -\frac{wh_{yx}(t)}{m_y}y_1(t) - \left(\omega_{ny}^2 + \frac{wh_{yy}(t)}{m_y}\right)y_2(t) - 2\zeta_y\omega_{ny}y_4(t) + \frac{wh_{yx}(t)}{m_y}y_1(t-\tau) + \frac{wh_{yy}(t)}{m_y}y_2(t-\tau) \quad (22d)$$

It is seen that equation (22a-22d) is the four-dimensional state space form written in compact form as

$$\dot{y}(t) = \mathbf{A}(t)y(t) - \mathbf{B}(t)y(t-\tau) \quad (23)$$

Where $y(t) = \{y_1(t) \quad y_2(t) \quad y_3(t) \quad y_4(t)\}^T$ (the superscript "T" means transposition)

$$\mathbf{A}(t) = \begin{bmatrix} 0 & 0 & 1 & 0 \\ 0 & 0 & 0 & 1 \\ -\omega_{nx}^2 - \frac{wh_{xx}(t)}{m_x} & -\frac{wh_{xy}(t)}{m_x} & -2\zeta_x\omega_{nx} & 0 \\ -\frac{wh_{yx}(t)}{m_y} & -\omega_{ny}^2 - \frac{wh_{yy}(t)}{m_y} & 0 & -2\zeta_y\omega_{ny} \end{bmatrix} \quad (24)$$

$$\boldsymbol{B}(t) = \begin{bmatrix} 0 & 0 & 0 & 0 \\ 0 & 0 & 0 & 0 \\ -\frac{wh_{xx}(t)}{m_x} & -\frac{wh_{xy}(t)}{m_x} & 0 & 0 \\ -\frac{wh_{yx}(t)}{m_y} & -\frac{wh_{yy}(t)}{m_y} & 0 & 0 \end{bmatrix} \quad (25)$$

Equation (23) is then re-arranged by splitting matrix $\mathbf{A}(t)$ into $\mathbf{B}(t)$ and a constant matrix $\mathbf{A}$ so that the governing model can conform with the full-discretization method such that equation (23) becomes

$$\dot{y}(t) = \mathbf{A}y(t) + \mathbf{B}(t)y(t) - \mathbf{B}(t)y(t-\tau) \quad (26)$$

where

$$\mathbf{A} = \begin{bmatrix} 0 & 0 & 1 & 0 \\ 0 & 0 & 0 & 1 \\ -\omega_{nx}^2 & 0 & -2\zeta_x\omega_{nx} & 0 \\ 0 & -\omega_{ny}^2 & 0 & -2\zeta_y\omega_{ny} \end{bmatrix} \quad (27)$$

The procedure which involves discretizing the system's period and interpolating or approximating the solution in the discrete intervals is adopted for this work. The full-discretization method is the choice of stability analysis in this work because it has been proven to save more computational time than the semi-discretization method. This is due to the introduction of interpolation polynomials in the integration scheme of full-discretization method which upon solving produces a discrete map that is used for stability analysis. The full-discretization method is heavily based on discretization. The discretization and solution schemes are summarized from the work [18] to involve dividing the period of the governing full-discretization model (equation (26)) $\tau$ into $r$ equal discrete time intervals $[t_i, t_{i+1}]$ where $i = 0, 1, 2, \ldots\ldots\ldots (r-1)$ and $t_i = i\frac{\tau}{r} = i\Delta t = i(t_{i+1} - t_i)$.

Equation (26) is then handled as the governing model in the general discrete interval $[t_i, t_{i+1}]$. The solution in the discrete interval $[t_i, t_{i+1}]$ arises from definite integration between the limits $t_i$ and $t_{i+1}$ to become

$$\mathrm{y}_{i+1} = \mathrm{e}^{\mathrm{A}\Delta t}\mathrm{y}_i + \int_{t_i}^{t_{i+1}} e^{A(t_{i+1}-s)}[\mathrm{B}(s)y(s) - \mathrm{B}(s)y(s-\tau)]\mathrm{d}s \tag{28}$$

What differentiates various full-discretization methods is the manner of proceeding from equation (28). The original full-discretization method [17] approximated the milling solution or motion $y(s)$ with the tool of linear interpolation theory. Other subsequent full-discretization methods which are seen in the reference list of the work [18] are also based on interpolation theory of various orders and kinds (i.e, Lagrange, Newton and Hermite interpolation theories). The work [18] has introduced full-discretization methods for which the milling motion $y(s)$ is approximated with least squares theory to yield considerable savings in computational time. The first-order least squares approximation of the state terms $y(s)$, $B(s)$ and $y(t-\tau)$ is as follows

The first order least squares approximation of the state term $y(s)$ is seen as

$$y(s) = \{1\ s\}\left[\sum_{l=i}^{i+1}\begin{Bmatrix}1\\ s_l\end{Bmatrix}\{1\ s\}\right]^{-1}\sum_{l=i}^{i+1}\begin{Bmatrix}1\\ s_l\end{Bmatrix}y_l \tag{29}$$

It should be noted that $l = i$ and $l = i+1$ in the summation signs of equation (29) corresponding to terms at $t_i$ and $t_{i+1}$. This is re-written as

$$y(s) = \{1\ s\}\begin{bmatrix}\sum_{\mathrm{l=i}}^{\mathrm{i+1}}1 & \sum_{l=i}^{i+1}s_l\\ \sum_{l=i}^{i+1}s_l & \sum_{l=i}^{i+1}s_l^2\end{bmatrix}^{-1}\begin{Bmatrix}\sum_{l=i}^{i+1}y_l\\ \sum_{l=i}^{i+1}s_l y_l\end{Bmatrix} \tag{30}$$

Equation (30) is further re-written as

$$y(s) = \frac{\{1s\}}{\sum_{i=l}^{i+1}1\sum_{i=l}^{i+1}s_l{}^2 - \left(\sum_{l=i}^{i+1}s_l\right)^2}\begin{bmatrix}\sum_{\mathrm{l=i}}^{\mathrm{i+1}}s_l{}^2 & -\sum_{l=i}^{i+1}s_l\\ -\sum_{l=i}^{i+1}s_l & \sum_{l=i}^{i+1}1\end{bmatrix}^{-1}\begin{Bmatrix}\sum_{l=i}^{i+1}y_l\\ \sum_{l=i}^{i+1}s_l y_l\end{Bmatrix} \tag{31}$$

The above equation is multiply to give

$$y(s) = \frac{\sum_{l=i}^{i+1}s_l{}^2\sum_{l=i}^{i+1}y_l - \sum_{l=i}^{i+1}s_l\sum_{l=i}^{i+1}s_l y_l}{\sum_{i=l}^{i+1}1\sum_{i=l}^{i+1}s_l{}^2 - \left(\sum_{l=i}^{i+1}s_l\right)^2} + \frac{-\sum_{l=i}^{i+1}s_l\sum_{l=i}^{i+1}y_l + \sum_{l=i}^{i+1}1\sum_{l=i}^{i+1}s_l y_l}{\sum_{i=l}^{i+1}1\sum_{i=l}^{i+1}s_l{}^2 - \left(\sum_{l=i}^{i+1}s_l\right)^2}s \tag{32}$$

By carrying out the summation in equation (32) and simplifying it gives equation (33a)

$$y(s) = \frac{t_{i+1}y_i - t_i y_{i+1}}{\Delta t} + \frac{-y_i + y_{i+1}}{\Delta t}s \tag{33a}$$

With the substitution of $t_i = 0$ and $t_{i+1} = \Delta t$, Equation (33a) is put in the form

$$y(s) = \frac{1}{\Delta t}(\Delta t - s)y_i + \frac{1}{\Delta t}s\,y_{i+1} \tag{33b}$$

In the same way as above, the delay state $y(s-\tau)$ and periodic coefficient matrix $B(t)$ will also give as

$$y(t-\tau) = \frac{1}{\Delta t}(\Delta t - t)y_{i-r} + \frac{1}{\Delta t}t\,y_{i+1-r} \tag{34}$$

$$B(s) = \frac{1}{\Delta t}(\Delta t - t)\mathbf{B}_i + \frac{1}{\Delta t}t\,B_{i+1} \tag{35}$$

Equations (33a), (34) and (35) are inserted into equation (28) to give

$$\mathrm{y}_{i+1} = F_0\mathrm{y}_i + (G_{11}\mathrm{B}_i + G_{12}\mathrm{B}_{i+1})\mathrm{y}_i + (G_{12}\mathrm{B}_i + G_{13}\mathrm{B}_{i+1})\mathrm{y}_{i+1} - (G_{11}\mathrm{B}_i + G_{12}\mathrm{B}_{i+1})\mathrm{y}_{i-r} - (G_{12}\mathrm{B}_i + G_{13}\mathrm{B}_{i+1})\mathrm{y}_{i+1-r} \quad (36)$$

Where

$$G_{11} = \frac{1}{(\Delta t)^2}\{F_1(\Delta t)^2 - 2F_2\Delta t + F_3\} \quad (36a)$$

$$G_{12} = \frac{1}{(\Delta t)^2}\{F_2\Delta t - F_3\} \quad (36b)$$

$$G_{13} = \frac{1}{(\Delta t)^2}F_3 \quad (36c)$$

$$F_0 = \mathrm{e}^{\mathrm{A}\Delta t} \quad (37a)$$

and

$$F_1 = \int_{t_i}^{t_{i+1}} e^{A(t_{i+1}-s)}\mathrm{d}s = \int_0^{\Delta t} e^{A(\Delta t-s)}$$

$$ds = \left\{e^{A\Delta t} - e^{A(\Delta t-s)}\right\}_0^{\Delta t}, F_1 = (F_0 - \mathrm{I})\mathrm{A}^{-1} \quad (37b)$$

$$F_2 = \int_{t_i}^{t_{i+1}} e^{A(t_{i+1}-s)(s-\mathrm{t_i})}\mathrm{d}s$$

$$ds = \int_0^{\Delta t} e^{A(\Delta t-s)}\mathrm{s}ds = \left\{-se^{A(\Delta t-s)}\mathrm{A}^{-1} + \mathrm{e}^{\mathrm{A}\Delta t}(\mathrm{A}^{-1})^2 - e^{A(\Delta t-s)}(\mathrm{A}^{-1})^2\right\}_0^{\Delta t}$$

$$F_2 = (F_1 - \Delta\Delta t\mathrm{I})\mathrm{A}^{-1} \quad (37c)$$

$$F_3 = \int_{t_i}^{t_{i+1}} e^{A(t_{i+1}-s)(s-\mathrm{t_i})^2}\mathrm{d}s = \int_0^{\Delta t} e^{A(\Delta t-s)}\mathrm{s}^2\mathrm{d}s$$

$$= \left\{-\mathrm{s}^2e^{A(\Delta t-s)}\mathrm{A}^{-1} + \mathrm{se}^{\mathrm{A}\Delta t}(\mathrm{A}^{-1})^2 - se^{A(\Delta t-s)}(\mathrm{A}^{-1})^2\right\}_0^{\Delta t} + \left\{-se^{A(\Delta t-s)}(\mathrm{A}^{-1})^2 + \mathrm{e}^{\mathrm{A}\Delta t}(\mathrm{A}^{-1})^3 - e^{A(\Delta t-s)}(\mathrm{A}^{-1})^3\right\}_0^{\Delta t} - \{se^{A\Delta t}(\mathrm{A}^{-1})^2\}_0^{\Delta t} + \left\{\mathrm{e}^{\mathrm{A}\Delta t}(\mathrm{A}^{-1})^2 - e^{A(\Delta t-s)}(\mathrm{A}^{-1})^2\right\}_0^{\Delta t}$$

$$therefore, \quad F_3 = (2F_2 - (\Delta t)^2\mathrm{I})\mathrm{A}^{-1} \quad (37d)$$

The equation (36) is re-arranged to become

$$\mathrm{y}_{i+1} = \mathrm{P}_i(F_0 + G_{11}\mathrm{B}_i + G_{12}\mathrm{B}_{i+1})\mathrm{y}_i - \mathrm{P}_i(G_{12}\mathrm{B}_i + G_{13}\mathrm{B}_{i+1})\mathrm{y}_{i+1-r} - \mathrm{P}_i(G_{11}\mathrm{B}_i + G_{12}\mathrm{B}_{i+1})\mathrm{y}_{i-r} \quad (38)$$

Where

$$\mathrm{P}_i = [\mathrm{I} - G_{12}\mathrm{B}_i - G_{13}\mathrm{B}_{i+1}]^{-1} \quad (39)$$

The local discrete map derived from equation (38) is given by [15]

$$\begin{Bmatrix} \mathrm{y}_{i+1} \\ \mathrm{y}_i \\ \mathrm{y}_{i-1} \\ \vdots \\ \mathrm{y}_{i+1-r} \end{Bmatrix} = \begin{bmatrix} \mathrm{M}_{11}^i & 0 & \cdots & 0 & \mathrm{M}_{1r}^i & \mathrm{M}_{1,r+1}^i \\ \mathrm{I} & 0 & \cdots & 0 & 0 & 0 \\ 0 & \mathrm{I} & \cdots & 0 & 0 & 0 \\ \vdots & \vdots & \vdots & \vdots & \vdots & \vdots \\ 0 & 0 & 0 & 0 & \mathrm{I} & 0 \end{bmatrix} \begin{Bmatrix} \mathrm{y}_i \\ \mathrm{y}_{i-1} \\ \mathrm{y}_{i-2} \\ \vdots \\ \mathrm{y}_{i-r} \end{Bmatrix} \quad (40)$$

where

$$\mathrm{M}_{11}^i = \mathrm{P}_i(F_0 + G_{11}\mathrm{B}_i + G_{12}\mathrm{B}_{i+1}) \quad (41a)$$

$$\mathrm{M}_{1r}^i = -\mathrm{P}_i(G_{12}\mathrm{B}_i + G_{13}\mathrm{B}_{i+1}) \quad (41b)$$

$$\mathrm{M}_{1,r+1}^i = -\mathrm{P}_i(G_{11}\mathrm{B}_i + G_{12}\mathrm{B}_{i+1}) \quad (41c)$$

The stability matrix for the system becomes [15]

$$\psi = \mathrm{M}_{r-1}\mathrm{M}_{r-2}\ldots\ldots\mathrm{M}_0 \quad (42)$$

Where

$$\mathrm{M}_i = \begin{bmatrix} \mathrm{M}_{11}^i & 0 & \cdots & 0 & \mathrm{M}_{1r}^i & \mathrm{M}_{1,r+1}^i \\ \mathrm{I} & 0 & \cdots & 0 & 0 & 0 \\ 0 & \mathrm{I} & \cdots & 0 & 0 & 0 \\ \vdots & \vdots & \vdots & \vdots & \vdots & \vdots \\ 0 & 0 & 0 & 0 & \mathrm{I} & 0 \end{bmatrix} \quad (43)$$

The aim of the afore-conducted mathematical analysis is derivation of the stability matrix $\psi$. Utilizing the matrices in equations (36a-36c), (37a-37d), (39), (41a-41c) and (43) in the stability matrix of equation (42) is all that is needed for stability characterization of the system. This obviates the need to go through the mathematical rigorous of this chapter by any reader interested only in the stability matrix and stability computation. The nature of eigen-values of the stability matrix is the criterion for stability characterization of milling process. Asymptotic stability requires all the $2r + 2$ eigen-values of the stability matrix $\psi$ to exist within the unit circle centred at the origin of the complex plane [18]. Stability boundary of milling process is then a curve that joins the critical parameter combinations at which

maximum-magnitude eigen-values of ψ lie on the circumference of the unit circle [18]. Milling stability lobes are computed with a value of $r$ that is big enough to guarantee benchmark accuracy [19]. Computations in literature are normally computed on $n_\Omega$ by $n_w$ grid on the plane of spindle speed and axial depth of cut. Computations in this work will include computing on $n_\Omega$ by $n_b$ grid on the plane of spindle speed and radial depth of cut.

# 5. Algorithms for Computation of Stability Limits of Milling

Delineation of milling process into stable or unstable occasioned by chatter can only have a real, physical or numerical reality when the constant parameters (which include tool, prescription and cutting parameters) are known numerically. The knowledge of tool and cutting parameters can stem from either pure experimental analysis or hybrid of experimental and numerical/theoretical analysis [20, 22].

Stability limits of the milling process can be computed by calculation, sorting and mapping of the eigen-values of the stability matrix ψ given in equation (42). As stated earlier, stability limit of milling process is a curve that joins the critical parameter combinations at which maximum-magnitude eigen-values of ψ lie on the circumference of the unit circle. This means that stability limit is arrived at when all parameters combinations at which eigen-values of unit magnitude are calculated, sorted out and connected by a curve. Computations of milling stability limit in literature normally give axial depth of cut as a function of spindle speed at a given value of radial depth of cut. Numerical computations of milling stability limit in the next section will include giving radial depth of cut as a function of spindle speed at a given value of axial depth of cut and giving radial depth of cut as a function of axial depth of cut at a given value of spindle speed. The procedures for these computations are spelt out in the following algorithms.

**Algorithm 1**

The algorithm for computation of stability limits of milling giving axial depth of cut as a function of spindle speed at a fixed value of radial depth of cut which is based on the analytical development in previous sections is as follows;

1. Provide the values of tool and cutting parameters given. Also provide the approximation parameter $r$, radial immersion $\rho = b/D$, the step and number of steps of computation for both axial depth of cut and spindle speed.
2. Compute the time-invariant matrix A and its inverse.
3. Chose the first step of spindle speed and compute the discrete delay or period $\tau$, the discrete time step range $\Delta t = \frac{\tau}{r}$, the $F$ and G matrices.
4. Chose the first step of axial depth of cut with spindle speed fixed as chosen in 3 and form discrete time intervals $[t_i, t_{i+1}]$ where $i = 0, 1, 2, \ldots\ldots\ldots (r-1)$ and $t_i = i\frac{\tau}{r} = i\Delta t = i(t_{i+1} - t_i)$. At the extremities of the first discrete time interval $[t_0, t_1]$ compute $\theta_j(t)$, $g_j(t)$, $h_{xx}(t)$, $h_{xy}(t)$, $h_{yx}(t)$, $h_{yy}(t)$ and use the result to form the matrices $B(t_0)$ and $B(t_1)$. Use the G matrices together with the matrices $B(t_0)$ and $B(t_1)$ to form the matrix $P_0$. Then form the matrices $M_{11}^0$, $M_{1r}^0$ and $M_{1,r+1}^0$ from the G matrices, $F_0$, $B(t_0)$ and $B(t_1)$ and $P_0$. Making use of the matrices $M_{11}^0$, $M_{1r}^i$ and $M_{1,r+1}^0$ form the matrix $M_0$
5. Carry out the operation in algorithm step 4 $r-1$ times at the remaining steps $i = 1, 2, \ldots\ldots\ldots (r-1)$ and use result of all the steps to form the stability matrix ψ. Compute the eigen-values of ψ and chose the eigen-value with maximum magnitude.
6. Repeat steps 4 and 5 for the remaining steps of axial depth of cut.
7. Repeat steps 3-6 for the remaining steps of spindle speed.
8. Connect the parameter combinations of spindle speed and axial depth of cut at which maximum magnitude of eigen-values is unity to form the stability limit.

**Algorithm 2**

On the other hand the algorithm for computation of stability limits of milling that presents radial depth of cut (or radial immersion) as a function of spindle speed at a fixed value of axial depth of cut is as follows;

1. Provide the values of tool and cutting parameters given. Also provide the approximation parameter $r$, axial depth of cut, the step and number of steps of computation for both radial depth of cut and spindle speed.
2. Compute the time-invariant matrix A and its inverse.
3. Chose the first step of spindle speed and compute the discrete delay or period $\tau$, the discrete time step range $\Delta t = \frac{\tau}{r}$, the $F$ and G matrices.
4. Chose the first step of radial depth of cut with spindle speed fixed as chosen in 3 and form discrete time intervals $[t_i, t_{i+1}]$ where $i = 0, 1, 2, \ldots\ldots\ldots (r-1)$ and $t_i = i\frac{\tau}{r} = i\Delta t = i(t_{i+1} - t_i)$. At the extremities of the first discrete time interval $[t_0, t_1]$ compute $\theta_j(t)$ and utilize it together with the chosen radial depth of cut to compute $g_j(t)$ then compute $h_{xx}(t)$, $h_{xy}(t)$, $h_{yx}(t)$, $h_{yy}(t)$ and use the results to form the matrices $B(t_0)$ and $B(t_1)$. Use the G matrices together with the matrices $B(t_0)$ and $B(t_1)$ to form the matrix $P_0$. Then form the matrices $M_{11}^0$, $M_{1r}^0$ and $M_{1,r+1}^0$ from the G matrices, $F_0$, $B(t_0)$ and $B(t_1)$ and $P_0$. Making use of the matrices $M_{11}^0$, $M_{1r}^i$ and $M_{1,r+1}^0$ form the matrix $M_0$.
5. Carry out the operation in the algorithm step4 $r-1$ times at the remaining steps $i = 1, 2, \ldots\ldots\ldots (r-1)$ and use result of all the steps to form the stability matrix ψ. Compute the eigen-values of ψ and chose the eigen-value with maximum magnitude.
6. Repeat steps 4 and 5 for the remaining steps of radial

depth of cut.

7. Repeat steps 3-6 for the remaining steps of spindle speed.
8. Connect the parameter combinations of spindle speed and radial depth of cut at which maximum magnitude of eigen-values is unity to form the stability limit.

**Algorithm 3**

Stability limits of milling on the plane of axial depth of cut and radial depth of cut at fixed spindle speed is generated by following the algorithm that follows;

1. Provide the values of tool and cutting parameters. Also provide the approximation parameter $r$, the fixed spindle speed, the step and number of steps of computation for both axial and radial depths of cut.
2. Compute the time-invariant matrix A and its inverse, the discrete delay or period $\tau$, the discrete time step range $\Delta t = \frac{\tau}{r}$ and the $F$ and G matrices.
3. Chose the first step of axial depth of cut then chose the first step of radial depth of cut. Form discrete time intervals $[t_i, t_{i+1}]$ where $i = 0, 1, 2, \ldots\ldots\ldots (r-1)$ and $t_i = i\frac{\tau}{r} = i\Delta t = i(t_{i+1} - t_i)$. At the extremities of the first discrete time interval $[t_0, t_1]$ compute $\theta_j(t)$ and utilize it together with the chosen radial depth of cut to compute $g_j(t)$ then compute $h_{xx}(t)$, $h_{xy}(t)$, $h_{yx}(t)$, $h_{yy}(t)$ and use the results to form the matrices $B(t_0)$ and $B(t_1)$. Use the G matrices together with the matrices $B(t_0)$ and $B(t_1)$ to form the matrix $\mathrm{P}_0$. Then form the matrices $\mathrm{M}_{11}^0$, $\mathrm{M}_{1r}^0$ and $\mathrm{M}_{1,r+1}^0$ from the G matrices, $F_0$, $B(t_0)$ and $B(t_1)$ and $\mathrm{P}_0$. Making use of the matrices $\mathrm{M}_{11}^0$, $\mathrm{M}_{1r}^i$ and $\mathrm{M}_{1,r+1}^0$ form the matrix $\mathrm{M}_0$.
4. With the axial depth of cut fixed at value in step4 carry out the operation in the algorithm step 4 $r-1$ times at the remaining steps $i = 1, 2, \ldots\ldots\ldots (r-1)$ and use result of all the steps to form the stability matrix $\psi$. Compute the eigen-values of $\psi$ and chose the eigen-value with maximum magnitude.
5. Repeat steps 3 and 4 for the remaining steps of radial depth of cut.
6. Repeat steps 3-6 for the remaining steps of axial depth of cut.
7. Connect the parameter combinations of axial and radial depths of cut at which maximum magnitude of eigen-values are unity to form the stability limit.

Each of the three presented algorithms above will be utilized to generate stability limits that will be jointly used to delineate the stability lobs diagram [22].

# 6. Results and Discussion

**Simulation of Stability Limits of Milling**

Stability limits from algorithms 1 and 2 are the ones that combine to give the spindle speed of productive depth of cut. Such spindle speeds, when ascertained are utilized in the algorithm 3 for generating of stability limit that allows selection of the maximum product $w\rho$ at which MRR may be maximized. The graphs of all the aforementioned algorithms are mapped out with MATLAB for stability milling process on three different plane of parameter space of the prescription parameters for comparative analysis.

Numerical values of parameters to be use in the stability analysis is borrowed from Weck et al as cited in [23] and are presented thus: $w_{nx} = 600HZ, w_{ny} = 660HZ$, $k_x = \frac{5600\,kN}{m}, k_y = \frac{5600\,kN}{m}, \zeta_x = 0.035,\ \zeta_y = 0.035,$ $m_x = {k_x}/{w_{nx^2}}, m_y = {k_y}/{w_{ny^2}},\ N = 3,\ C_t, C_n,\ \theta_s\ (up-millining)$. Where subscripts $x\ and\ y$ represents independent coordinates in $x\ and\ y$-directions respectively, $w_n$ is the natural frequency, $k$ is the stiffness, $\zeta$ is the damping ratio, $m$ is the modal mass, $N$ is the number of teeth on the milling tool, $\theta_s$ is the start angle of cut while $C_{t\ and}\ C_n$ represents tangential and normal cutting coefficients respectively.

Using parameters above and following algorithm 1 gives stability limits of milling on the plane of spindle speed and axial depth of cut at selected fixed radial immersions seen in figure 4 bellow.

It can be deduced from above figure that rise in radial immersion enhances the unstable region and suppresses the stable region which is as a result of chatter. This means that there is some kind of inverse relationship between the axial and radial depths of cut highlighting the need to determine the maximum value of their product for achieving maximized MRR thereby reducing the chatter in the milling process. The other important observation is that the peak axial depths of cut occasioned by the lobbing effects occur as fixed spindle speeds irrespective of value of the radial immersion. This observation is very useful for implementation of algorithm 3. It must be noted that figure 5b is validated by the figure generated with identical set of parameters in [24] meaning that algorithm 1 which is based on theoretical development in this work provides reliable stability limit of milling process.

When the same parameters are used in algorithm 2, it gives stability limits of milling on the plane of spindle speed and radial depth of cut at selected fixed axial depth of cut seen in Figure 5.

Figure 5 shares similar behaviour with Figure 4. It is seen in Figure 5 that rise in axial depth of cut enhances the unstable region and suppresses the stable region. This means that inverse relationship exists between the axial and limiting radial depths of cut thus highlighting the need to determine the maximum value of their product for achieving maximized MRR thereby reducing the chatter in the milling process. It is also seen that the peak radial depths of cut occasioned by the lobbing effects occur at fixed spindle speeds that are same as in figure 4 irrespective of value of the axial depth of cut. This observation which is consistent with figures 4 and 5 means that implementing algorithm 3 at any of such productive spindle speeds will generate the most

productive stability limits of milling on the plane of axial depth of cut and radial depth of cut. It must be noted that figure 5a is validated by the figure generated with identical set of parameters in [24] meaning that algorithm 2 which is based on theoretical development in previous sections of this work provides reliable stability limit of milling process.

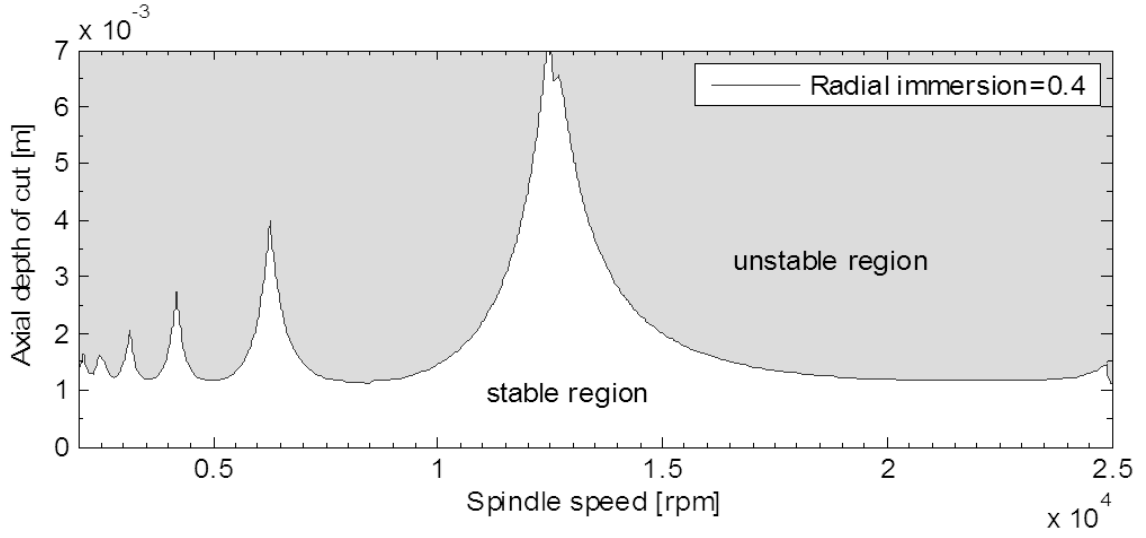


(a)

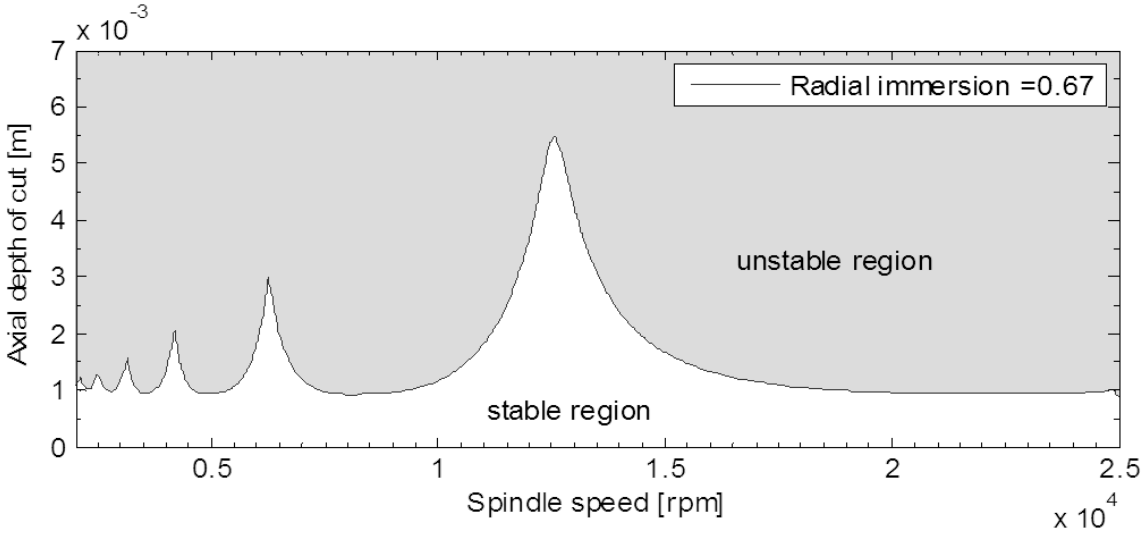


(b)

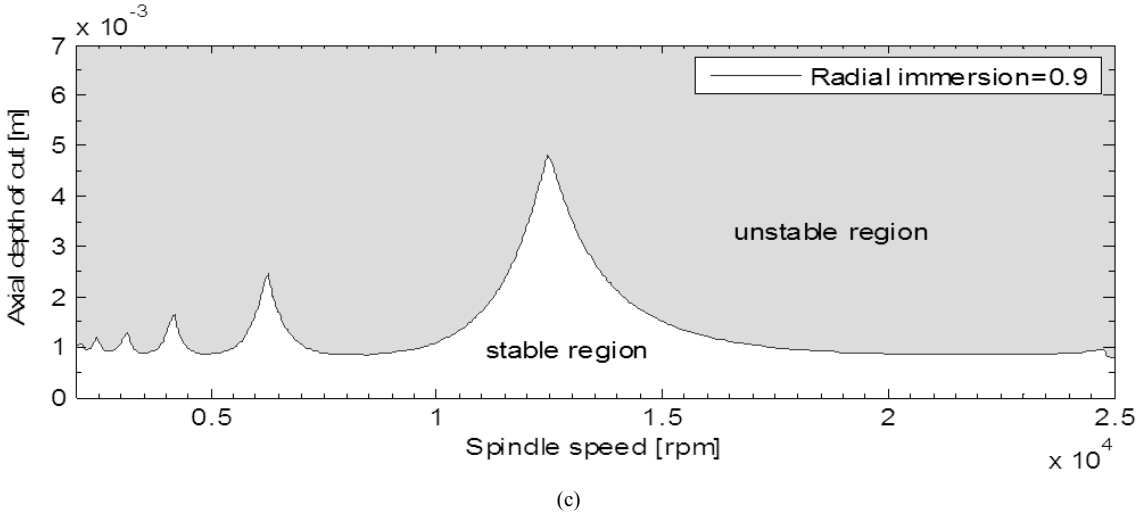


(c)

**Figure 4.** Stability Limits of Milling on the Plane of Spindle Speed and Axial Depth of Cut at Selected Fixed Radial Immersions

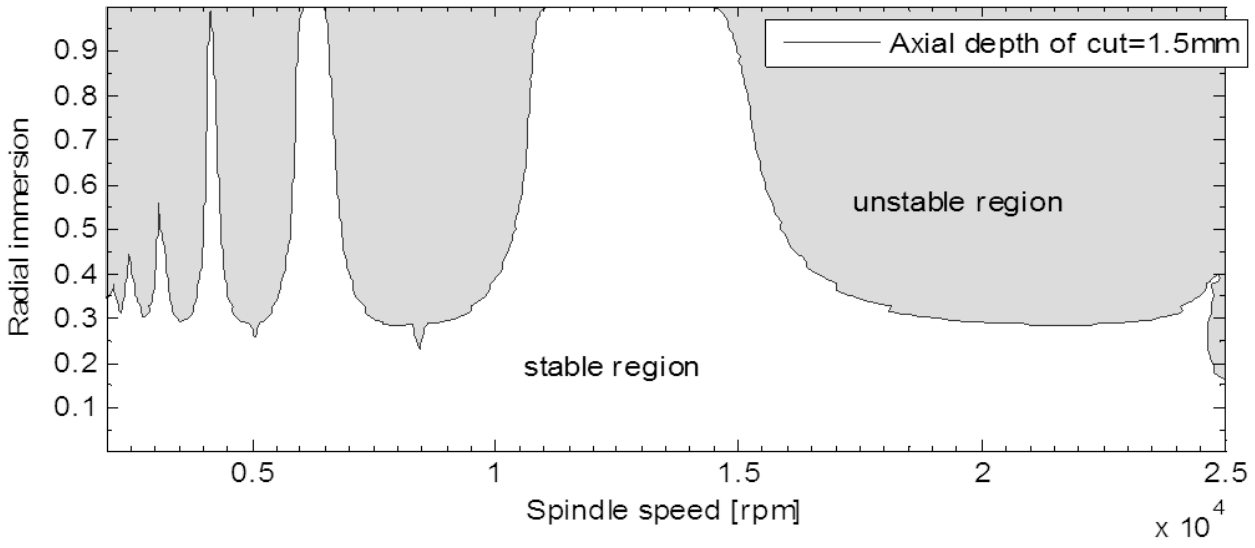


(a)

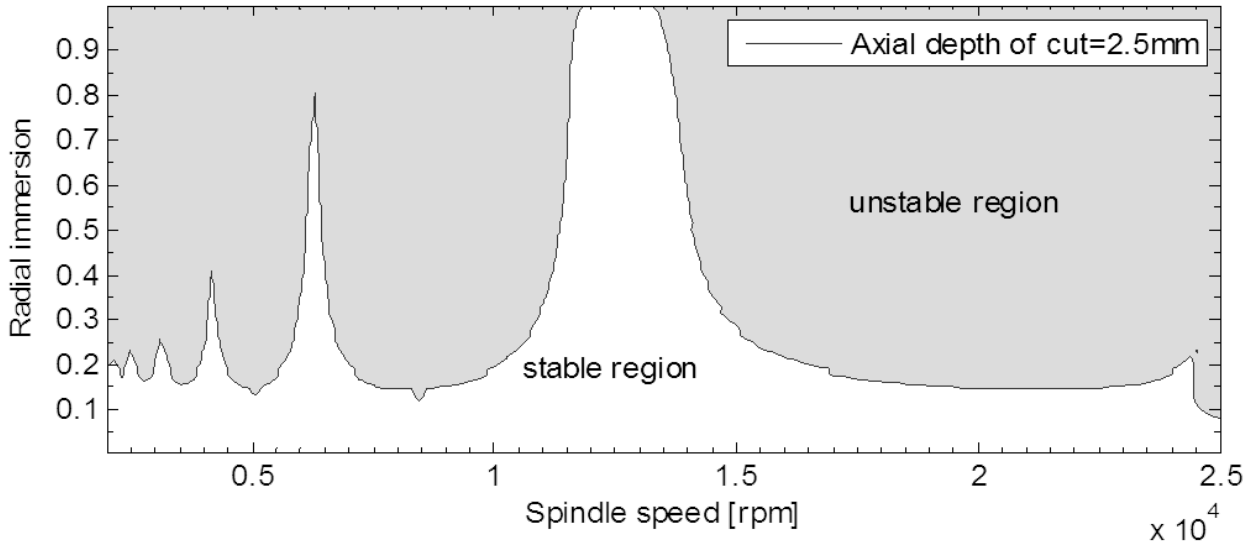


(b)

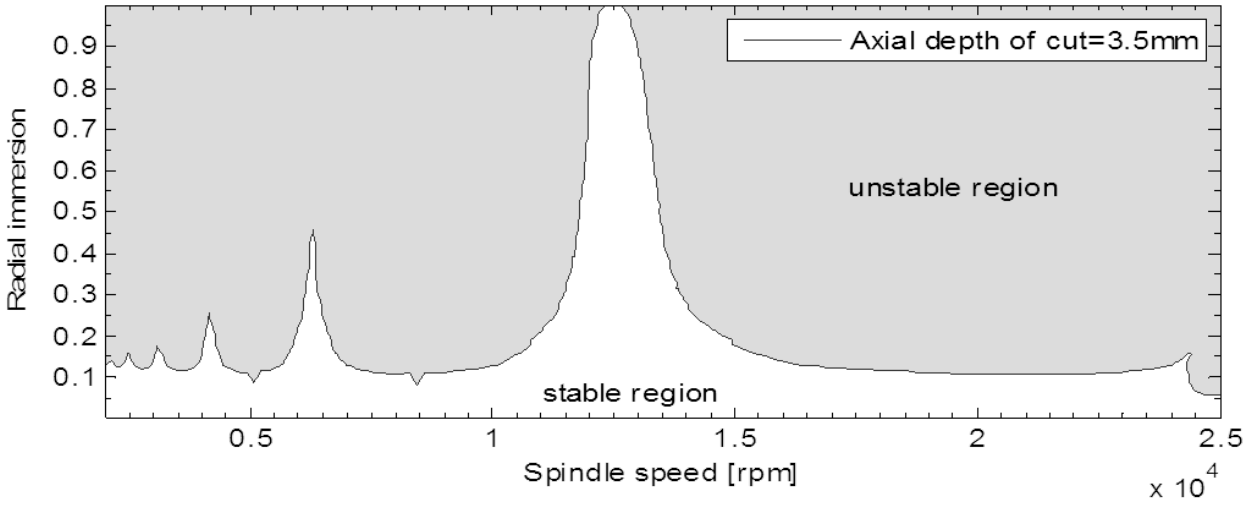


(c)

**Figure 5.** Stability limits of milling on the plane of spindle speed and radial depth of cut at selected fixed axial depths of cut

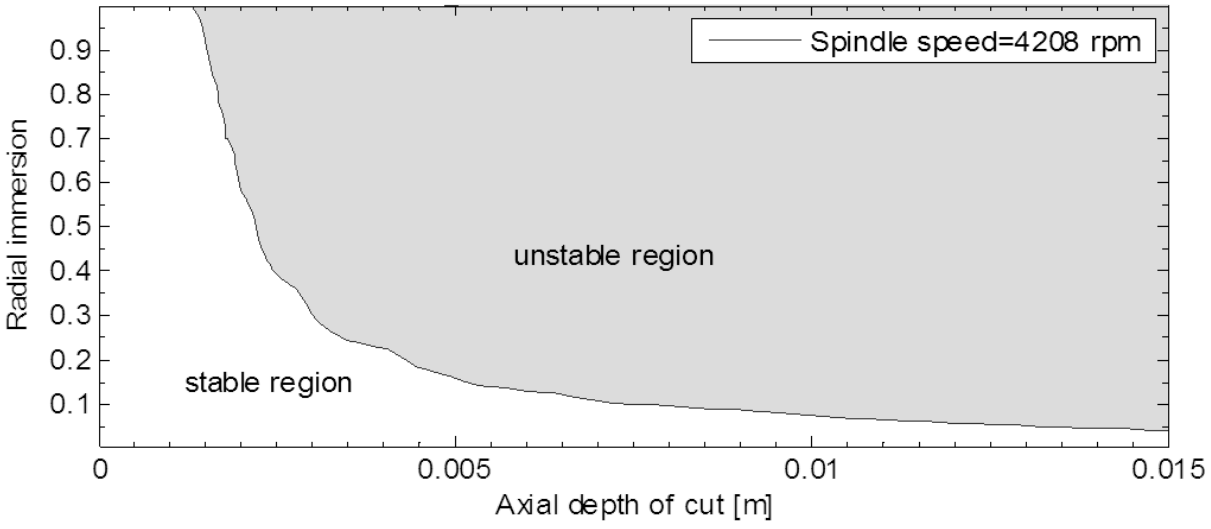


(a)

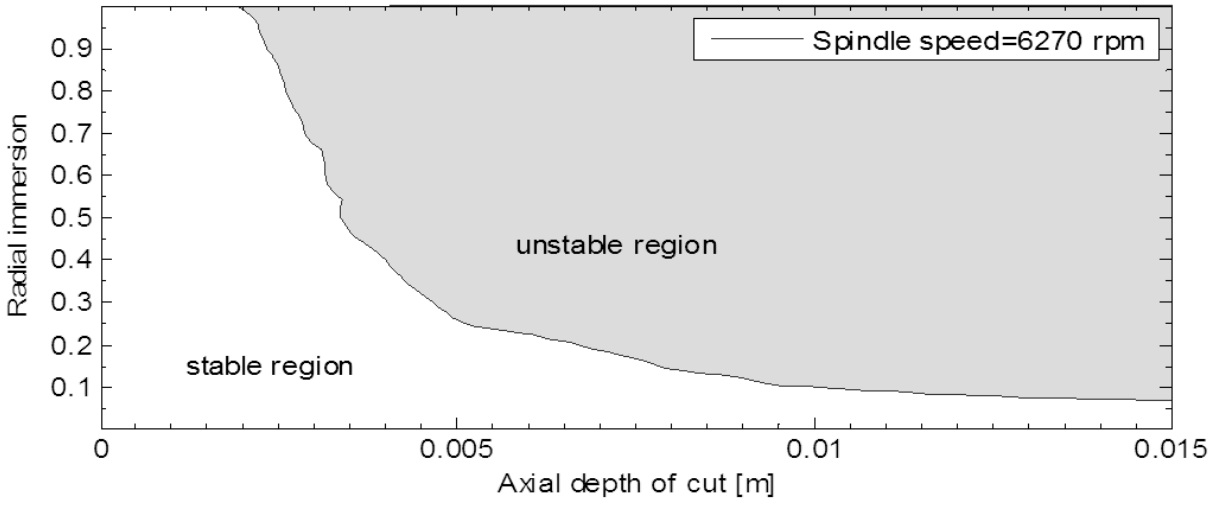


(b)

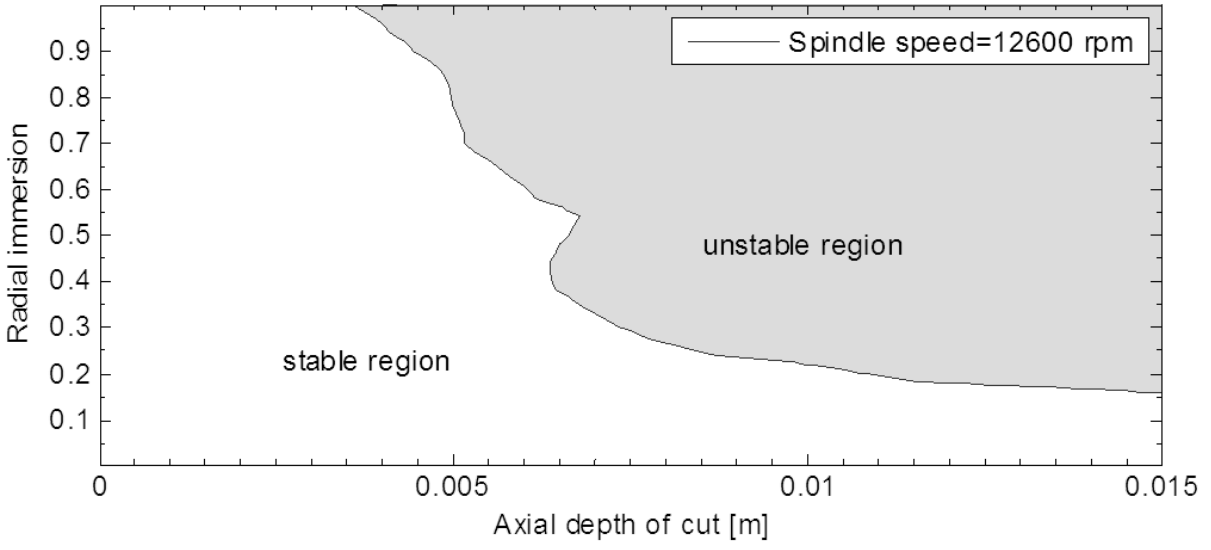


(c)

**Figure 6.** Stability limits of milling on the plane of axial depth of cut and radial depth of cut at selected productive spindle speeds

Using the same parameters above in algorithm 3, stability limits of milling on the plane of axial depth of cut and radial depth of cut at the selected productive spindle speeds 4208, 6270, 12600 were generated as seen in Figure 6.

The inverse relationship between limiting axial depth of cut and limiting radial depth of cut suggested by figures 4 and 5 is actually true looking at figure 6. It is seen in figure 6 that rise in spindle speed enhances the stable region and suppresses the unstable region. This means that for us to have chatter-free milling process, parameters like axial and radial depths of cut should be carefully selected together at high machining speed. It must be noted that figure 6c agrees closely with the figure generated with identical set of parameters in [24] meaning that algorithm 3 for the first order least squares approximated map of the work [18] provides reliable stability limit of milling process on the plane of depths of cut.

## 7. Conclusions

Regenerative chatter poses serious challenge to machine operator this days in achieving high accuracy and acceptable surface finish. Various methods are available for the control of chatter. Some are analytical, semi-analytical while others are experimental. Some of the results of this work can be identified to be new in the field optimal machining. The work lays the foundation for use of the least squares approximated full-discretization method in stability analysis on the plane of axial depth of cut and radial depth of cut using analytical method. A detailed computational algorithm was presented for the purpose of delineating stability lobe diagram into stable and unstable regions. The stability lobe diagram if well understood, will be a guide to operators in selecting a chatter free spindle speed and depths of cut knowing that there are some spindle speed that are not productive and also the proper combination of the depths of cut so as to boost surface finish and greater accuracy.

## REFERENCES


[1] Osueke C.O, Ezugwu C.A.K, Adeoye A.O (2015) Dynamic approach to optimization of material removal rate through programmed optimal choice of milling process parameters, part 1: validation of result with CNC simulation. International Journal of innovative research in Advanced Engineering, 2(5), 118-129.

[2] Okokpujie Imhade P., Okonkwo Ugochukwu C., Okwudibe Chinenye D. (2015) Cutting parameters effects on surface roughness during end milling of aluminium 6061 alloy under dry machining operation. International Journal of Science and Research, 4(7), 2030-2036.

[3] Altintas, Y., "Manufacturing Automation: Metal Cutting Mechanics, Machine Tool Vibrations, and CNC Design", 1st ed., Ed. Cambridge University Press, NY, USA, 2000.

[4] Okokpujie Imhade P., Okonkwo Ugochukwu C. (2015). Effects of cutting parameters on surface roughness during end Milling of aluminium under minimum quantity lubrication (MQL). International Journal of Science and Research, 4(5), 2937-2942.

[5] Tobias, S.A. (1965). Machine Tool Vibration. Blackie and Sons Ltd, 340-364.

[6] Tlusty, J. and Ismail, F. (1981). Basic Nonlinearity in Machining Chatter. Annals of the CIRP, 30:21–25.

[7] F. W. Taylor, "On the art of cutting metals", Transactions of the American Society of Mechanical Engineers, pp. 31–35, 1907.

[8] S.A. Tobias, Vibraciones en Maquinas-Herramientas, URMO, Spain, 1961

[9] J. Tlusty, M. Polacek, "The stability of machine tools against self-excited vibrations in machining", International Research in Production Engineering, pp.465–474. 1963.

[10] Ozoegwu C.G. & Ezugwu C. (2015). Minimizing pocketing time by selecting most optimized chronology of tool passes. International journal of advanced manufacturing technology, 79(1-4).

[11] Budak, E., & Altintas, Y. (1994). Peripheral millingconditions for improved dimensional accuracy. Int. J. Mach. Tools Manufact. 34 (7) 907–918.

[12] Quintana, G. and Ciurana, J. (2011). Chatter in machining processes: a review, International Journal of Machine Tools and Manufacture. International Journal of Machine tools and manufacture, 51 (5) 363–376.

[13] Budak, E., and Altintas, Y. (1998). Analytical Prediction of Chatter Stability in Milling - Part I: General Formulation, Part II: Application To Common Milling Systems. Trans. ASME Journal of Dynamic Systems, Measurement and Control, 20:22–36.

[14] Hashimoto, M., Marui, E., and Kato, S. (1996). Experimental research on cutting force variation during regenerative chatter vibration in a plain milling operation. International Journal of Machine Tools and Manufacture, 36 (10) 1073–1092.

[15] Sridhar R, Hohn RE and Long GW. (1968). General Formulation of the Milling Process Equation, ASME J. of Eng. for Ind, 90: 317-324.

[16] Ozoegwu, C. G., Omenyi, S. N., Ofochebe, S. M., and Achebe, C. H. (2013) Comparing up and Down Milling Modes of End-Milling Using Temporal Finite Element Analysis, Applied Mathematics 3(1) 1-11.

[17] Ding Y, Zhu LM, Zhang XJ, Ding H. (2010). A full-discretization method for prediction of milling stability. International Journal of Machine Tools and Manufacture, 50:502–509.

[18] Ozoegwu, C.G. (2014). Least squares approximated stability boundaries of milling process, International Journal of Machine Tools and Manufacture, 79, 24–30.

[19] Altintas, Y., and Budak, E. (1995). Analytical Prediction of Stability Lobes in Milling. Annals of the CIRP, 44(1): 357–362.

[20] Okonkwo U.C, Osueke C.O, Ezugwu C.A.K (2015)

Minimizing machining time in pocket milling based on optimal combination of the three basic prescription parameters. International Research Journal of Innovative Engineering, 1(4), pp. 12-34.

[21] Sridhar, R., Hohn, R.E., and Long, G.W. (1968). A Stability Algorithm for the General Milling Process. Trans. ASME Journal of Engineering for Industry, 90:330–334.

[22] Ezugwu, C.A.K (2015). Minimizing Pocketing Time by Programmed Optimal Choice of Stable Milling Process Parameters: Master of Engineering Thesis, Nnamdi Azikiwe University, Awka, PP. 42- 46.

[23] Tekeli, A. and E. Budak, Maximization of chatter-free material removal rate in end milling using analytical methods, Machining Science and Technology, 9:147–167.

[24] Meritt, H. E. (1965). Theory of self-excited machine–tool chatter. Transactions of the ASME Journal of Engineering for Industry, 87, 447–454.